TECHNICAL ARTICLE

Combining XRD and XRF analysis in one Rietveld-like fitting

M. Bortolotti,[1,a)] L. Lutterotti,[1] and G. Pepponi[2]
[1]*Dipartimento di Ingegneria Industriale, Università degli Studi di Trento, Italy*
[2]*Center for Materials and Microsystems, Fondazione Bruno Kessler, Trento, Italy*

(Received 16 October 2016; accepted 21 February 2017)

X-ray diffraction (XRD) and X-ray fluorescence (XRF) are widely used analytical techniques for materials characterization; the information they provide can be considered complementary, as the former is mostly used to obtain crystallographic information and analyze phase content, whereas the latter is sensitive to elemental composition. Many researchers and technologists working in a variety of application fields already use them together in some sort of a "combined" approach, by separately performing XRD and XRF data collection and analysis on the same sample and then comparing the analytical results obtained to integrate and complement the respective analytical information. In this work, we propose a true combined approach to merge both XRD and XRF data acquisition and analysis. Custom analytical X-ray instrumentation has been developed to perform the simultaneous data acquisition, by using a single X-ray source and dedicated detectors to collect the diffracted and fluorescent X-ray photons from the same sample volume. Additionally, a combined XRD/XRF data analysis methodology has been implemented by extending Rietveld based code to incorporate the full pattern fitting of XRF spectra starting from the phases instead of a simple matrix elemental composition. We report two analytical examples from different application fields to better illustrate the capabilities of the proposed approach.
[doi:10.1017/S0885715617000276]

Key words: X-ray diffraction, X-ray fluorescence, combined analysis, quantitative phase analysis, Rietveld method

I. INTRODUCTION

X-ray diffraction (XRD) and X-ray fluorescence (XRF) represent two versatile non-destructive analytical techniques, widely adopted in both the engineering and scientific field. XRD is mostly used to perform structural and crystallographic characterization of polycrystalline mixture, including – but not limited to – phase identification and quantification, microstructure and texture analysis, *ab initio* structure determination. XRF, on the other hand, is mostly suited for accurate quantitative chemical characterization of materials. While from the theoretical point of view the information obtained from an XRD analysis implicitly embeds also the full chemical characterization of the sample, in reality several practical limitations suggest this is not the case. First of all, sensitivity to the presence of different elements in the same crystal structure mostly depends on the difference in atomic scattering factors and mean atomic radii, which are reflected in relative peak intensities and positions; for similar atomic species those can be quite small, leading to significant error in elemental quantification. In addition, the presence of amorphous fractions, which are not accurately quantifiable by XRD, can be obviously problematic for the accurate quantification of total chemical composition. It should be clear, thus, that an accurate independent chemical quantification, as that obtained from XRF, can be effectively used to correct and guide the quantitative characterization of the sample performed by means of XRD; in addition, an independent chemical characterization of the sample can also be used in the initial stage of phase identification, which is often ambiguous when based only on the peak positions and intensities obtained from the diffractogram. Conversely, results obtained from XRD can be used to complement missing or incomplete information coming from an XRF analysis; first of all, the presence of light-elements or, in general, elements outside the sensitivity range of XRF technique can be indirectly ascertained by recognizing the presence of the corresponding elements-bearing phases. In addition, by taking into account a full crystallographic model in place of a simple list of elements, it is possible to perform a more reliable modeling of the matrix effect. In principle, the true absorption factors can be computed by having a direct measurement of the density from the crystallography and elemental composition of the phases.

For those reasons, it is clear that XRD and XRF techniques have to be considered as strongly complementary techniques in the amount and type of information obtainable; it appears thus quite natural to try to combine them from both an experimental and analytical point of view. As far as the first point goes, it has to be noted that in some of the relevant literature works dealing with the combined approach, diffraction and fluorescence signals are often acquired on different instruments (Pantos *et al.*, 2005; Schönenberger *et al.*, 2012). This has the advantage that the best experimental setups in term of radiation, sample conditioning and detectors can be adopted for the different techniques; however, by using different radiation sources, different sample volumes are being measured, possibly leading to incongruent results,

[a)]Author to whom correspondence should be addressed. Electronic mail: mauro.bortolotti@unitn.it

unless when dealing with perfectly homogenous samples. A different experimental approach is the use of some kind of integrated instrumentation, in which at least the radiation source is common for both techniques (Kerner *et al*., 1995; Vaniman *et al*., 1999; De Voorde *et al*., 2015). In this case, the interested volume from the incident beam is the same, but for the fluorescence the lower energy lines signal is coming mainly from the upper layers because of the absorption. In this work, we decided to adopt this latter approach, as this offers a clear practical advantage as well as a stronger theoretical foundation for the combined analysis methodology, as described in the rest of the paper.

Moreover, in the vast majority of the combined analysis literature work, the integration is limited to the experimental step, whereas the analytical step is performed independently for each technique, with the analytical results compared only at the end of the analysis, possibly in an iterative fashion (Schönenberger *et al*., 2012). In our work, we follow a novel approach, in which a single parametric model, describing a multi-phase polycrystalline mixture, is adopted to fit both the XRD and XRF data.

II. EXPERIMENTAL

To ensure a coherent data collection setup, with both XRD and XRF experimental signals coming from the same sample volume as previously illustrated, a custom X-ray instrument was implemented starting from an INEL Equinox 3500 XRD system (Figure 1). As a radiation source, a single Mo anode microfocus X-ray configuration was chosen as an optimal compromise for the two techniques; indeed, while a Cu anode source is often considered more convenient for XRD measurements, from an XRF standpoint it would have been too limited in terms of the sensitivity for the K lines of elements heavier than Co and L lines heavier than Dy. In the present iteration of the instrument we have chosen to keep the incident beam non-monochromatized or filtered to use the Bremsstrahlung high-energy part to excite more fluorescence lines and detect heavier elements. Instead a Zr filter with a thickness of 120 μm is placed in diffracted beam just before the corresponding detector.

For the signal acquisition part, a double detector configuration was chosen; despite working single detector implementations have been demonstrated for specific use cases (Vaniman *et al*., 1999), we think that the current relative technologies (e.g., photon counting two-dimensional (2D) CCDs (charge-coupled devices) or 2.5D hybrid pixel detectors) do not offer any significant advantage for laboratory instrumentation, while at the same time forcing excessive compromises on signal quality, resolution and speed. Thus, a IMXPAD s10 2D detector was adopted for the XRD part, operating in step-scanning mode on the second θ-axis, whereas an Amptek X123 silicon drift detector in fixed position (nearly orthogonal to the sample) was chosen for the XRF data acquisition part; both detectors offer good performances in terms of resolution and speed in their respective operating modes. The pixel size of the ImXPad is relatively large ($130 \times 130\ \mu m^2$ pixels), but collecting the curved diffraction rings in both directions effectively improves the resolution with respect to a linear detector having such resolution only along one direction.

For the data collection of each experiment, the second θ-axis, carrying the diffraction detector, is moved in step scanning mode, so that for each acquisition step a 2D diffraction image is acquired and then merged obtaining a Debye–Scherrer-like diffractogram, which is then integrated along the diffraction rings into the final 1D pattern. In addition, an XRF spectrum is collected every few scanning steps (typically every 1° in 2θ); this offers also the possibility of evaluating concentration gradients along the sample z-axis, when moving the first θ-arm carrying the source in a Bragg–Brentano-like geometry, by varying the penetration depth of the incident radiation.

Finally, a flexible four-axis sample holder setup (visible in the lower part of Figure 1) was implemented, allowing both standard powders as well as bulk samples to be positioned and aligned, as well as the possibility to perform mappings of inhomogeneous sample surfaces and spinning the sample around its normal axis. In Figure 1 among the detectors, an INEL CPS 120 curved detector is visible, but was not connected and used at the time of these experiments. Such detector is useful for quick measurements and sample mapping when no in-depth checking is required.

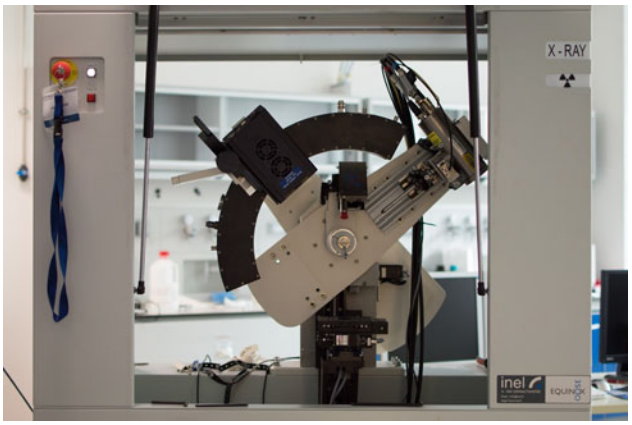

Figure 1. X-ray instrumentation for the combined data acquisition; an INEL Equinox 3500 diffractometer was adopted as a starting base for the development.

III. ANALYTICAL MODELING

The principal aspect that qualifies the novelty of the proposed methodology with respect to the current "combined analysis" literature is the simultaneous fitting of both the XRD and XRF data starting from a common structural model. This analytical approach has been implemented in the program Maud (Lutterotti *et al.*, 2007; Lutterotti, 2010) deriving the XRF implementation from the GimPy and JGIXA programs (Ingerle *et al.*, 2016).

To simultaneously fit XRD and XRF data, a comprehensive radiation–matter interaction model is adopted, taking into account both elastic scattering and photoelectric absorption/fluorescence. In the most general case, the sample is described as a multilayer, each layer containing a specific composition of crystallographic phases. The phase quantities in each layer, the elemental composition of each phase, and the distribution of the phases within each layer are modeled in order to reproduce both the XRD and XRF patterns. For the XRD, as in a Rietveld computation, the crystal structure is used and additional element and/or impurities are inserted as substitutional

https://doi.org/10.1017/S0885715617000276 Published online by Cambridge University Press

atoms with partial site occupation. In some cases, some impurities may occupy more than one site and or substitute different atoms in different phases. In such cases some arbitrary assumptions must be made based on the chemistry and when not possible we distribute such impurities over all the possible phases.

By the model, the elemental composition of each layer and the associated matrix effects are used to compute the XRF spectra, taking into account the varying angle of the incident beam during the measurement and all filters or media encountered, to correctly model the different absorption path of the excited fluorescence photons traveling to the detector.

For the case of our instrument configuration, being the incident beam was not monochromatized or filtered, we need to account for all the energies and their spectral distribution. For this purpose, the model of Ebel (1999) is used to calculate the spectrum generated by the Mo microsource. Subsequently all elements (filters etc.) encountered along the path and up to the detector in the case of the XRD are used to calculate the spectral modification. Computation time increases considerably with respect to a monochromatic radiation especially in the case of diffraction, where a smaller energy resolution (0.05 keV instead of 1 keV for XRF) in the calculation has to be used to obtain smooth peak profile. As it will be evident in the figures with the diffraction fitting, the part of the Bremsstrahlung between 10 and 16 keV is less efficiently filtered by the Zr foil and gives rise to a high and long tail on the higher angle side of the diffraction peaks.

The simulated XRD and XRF datasets are then fitted against their experimental counterpart; this is performed, in a similar way to the classical Rietveld method (Rietveld, 1967, 1969), by optimizing the relevant parameters describing the structural model by means of a least-squares optimization; the corresponding combined fitness function can be written as:

$$\mathrm{WSS} = \sum_n k_n \mathrm{WSS}_n = \sum_n k_n \sum_i w_i \left(I_{i,n}^{\mathrm{calc}} - I_{i,n}^{\mathrm{exp}}\right)^2 \qquad (1)$$

where the summation over n concern the different techniques (XRD and XRF in this paper), k_n are the weights to be applied between techniques to balance their contribution in the fitting and the summation over i is the usual summation over all data of the pattern of each technique to obtain the weighted sum of squares to be minimized and w_i the statistical weights of each experimental point. In our case, we used for them the usual $w_i = 1/I_i^{\mathrm{exp}}$.

An important aspect of this procedure consists in setting the right balance between the diffraction and fluorescence data weights in the least-squares fitting. XRF spectra generally display higher intensities and thus better signal to noise ratio and, since several spectra are acquired for each XRD pattern, this ensures a significant statistical reliability. In the least squares refinement strategy, it is a good practice to increase the weight of the diffraction pattern contribution in order to establish a first qualitative estimation of the phase content. Once the main phases have been identified, modeling can shift to a more balanced situation, in which XRD and XRF data have comparable statistical weights. The weighting balance between XRD and XRF, in our opinion, should be judged case by case depending on the quality of the data in one with respect to the other and the information contained and needed. In the examples below, the final fitting is performed by adjusting the k_n weight of the XRF part to achieve nearly the same WSS as for the XRD despite the bigger number of spectra. This ensures a balanced fitting between the two parts. At this stage, with higher accuracy and precision, the elemental composition in each phase can be refined. In general, the analysis needs to proceed iteratively with the constant user supervision for what concerns the refined parameter selection, in a similar manner to a classical Rietveld refinement.

IV. APPLICATION EXAMPLES

To demonstrate the validity of the previously described combined XRD/XRF methodology, from both the experimental and analytical point of view, we provide here two application examples, respectively from the industrial quality control and material science fields.

The first application example refers to the quantitative characterization of ceramic industry waste. Both XRD and XRF, applied independently, can offer a great deal of information on such kind of sample, covering, however, only a partial aspect of the needed quantitative characterization. XRF for example, while offering an accurate quantification of most of the chemical elements in the sample, cannot provide the essential information about the sample crystallography; XRD, on the other hand, it is able to detect even the presence of light element-bearing phases, but in general is not nearly as accurate for a quantitative chemical analysis; also in the case of amorphous phases (a very common situation when dealing with ceramic samples) XRD cannot provide reliable quantitative information. For these reason, this seems like an ideal analytical example to demonstrate the power of the integrated approach.

To validate the procedure, XRD and XRF data were collected on the combined instrument previously described operating in a θ–θ reflection geometry. A preliminary XRF semi-quantitative analysis was performed to obtain the most significant elements in the sample; this information was then used to help the crystalline phase identification in the XRD data (*search match*). Dolomite, calcite and quartz where found as constituent phases; however, additional trace elements in addition to Ca, C, O, Mg and Si were detected in the XRF spectrum, namely Fe and K, which could not be directly accounted for by the phases recognizable in the diffraction data. Thus, Fe and K were interpreted as substitutional impurities of Ca atoms in dolomite (as the predominant phase) and modeled as such in the Maud (Lutterotti *et al.*, 2007; Lutterotti, 2010) software. Since a standard XRD-only Rietveld modeling did not offer the sensitivity to refine the occupancy factor of these impurities, a combined XRD/XRF fitting was performed as described in the previous section, with the crystallographic phases weight fractions as well as the occupancy factors of the substitutional impurities defined as refinable parameters of the combined model; this allowed to fit both the XRD diffractogram and the XRF spectrum using the same sample model, and to obtain reliable quantitative information for both the chemical and the crystallographic part. The final results are reported in Table I, the R factors are reported separately for each technique in the respective Figures 2 and 3.

The second application example refers to the characterization of a kaolin mineral (rich in kaolinite) powder sample used

https://doi.org/10.1017/S0885715617000276 Published online by Cambridge University Press

TABLE I. Chemical and crystallographic quantitative analysis for the ceramic industry waste sample.

Phase		Dolomite			Calcite			Quartz		
wt%		96.3(3)			3.0(1)			0.7(1)		
Element	O	Ca	C	Mg	Al	Fe	Si	K	Mn	Sr
wt%	51.4	21.5(1)	12.8	12.6	0.72	0.49(1)	0.33	0.18(3)	0.01(1)	0.02(1)

It is not possible to calculate the errors for the elements below the silicon as their quantity is estimated from the crystallography of the phases.

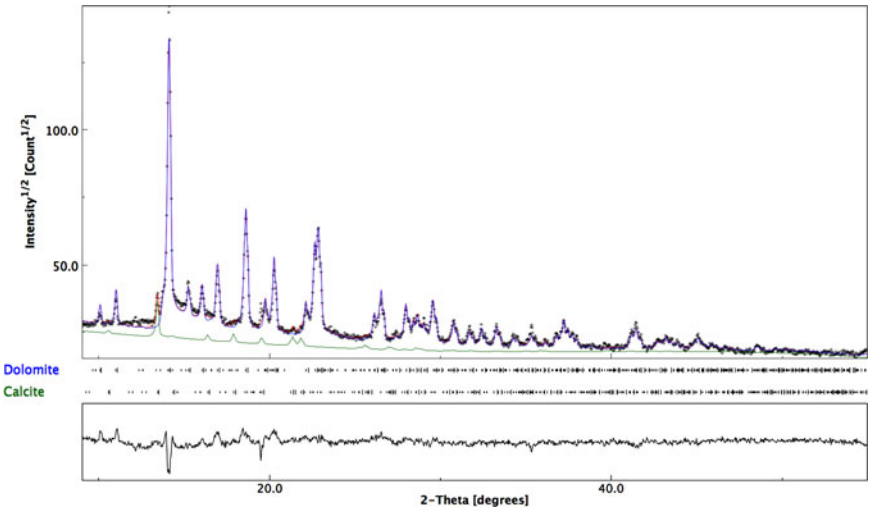

Figure 2. XRD fit for the ceramic industry waste example, showing total modeled diffraction pattern as well as the minor Calcite phase contribution (green line). R_{wp}: 8.5%.

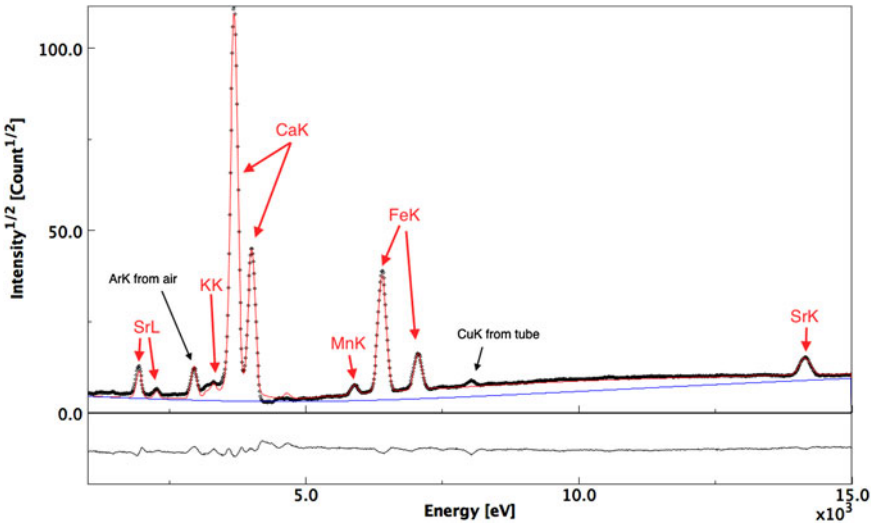

Figure 3. Full-pattern XRF fit for the ceramic industry waste example, showing relevant element peaks. R_{wp}: 15.1%. The R_{wp} factor is not too low because the fitting is cumulative for 40 spectra at different beam incident angle. However, the fit model had very few parameters with respect to the total number of data.

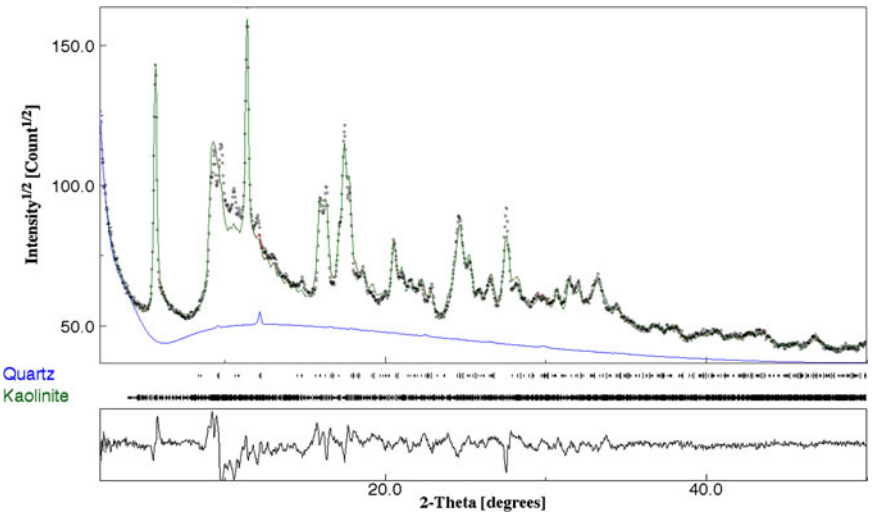

Figure 4. XRD fit for kaolinite sample. A small percentage of Quartz is visible. All reflections generated by the supercell Ufer single-layer model are shown. R_{wp}: 7.8%.

https://doi.org/10.1017/S0885715617000276 Published online by Cambridge University Press

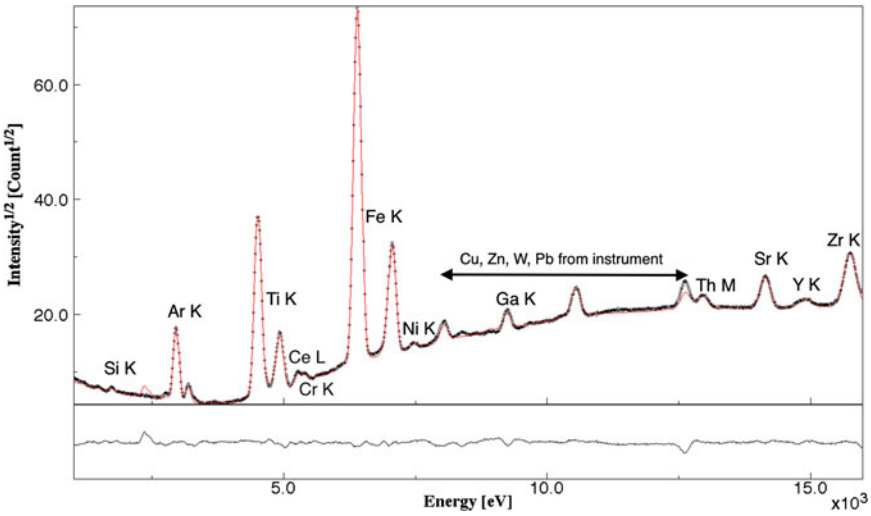

Figure 5. Full pattern XRF fit for kaolinite, showing relevant element peaks both from the sample and some spurious lines coming from part of the instrument such as lead shields on the collimator, brass (Cu, Zn) lines from the shutter passing through the collimator and arriving to the detector by diffraction. We take full advantage of a non-monochromatic beam to increase the number of detectable lines. With a monochromatic Mo radiation, it would have been impossible to see Zr lines. R_{wp}: 11.4% (40 spectra cumulative).

as filler in polymer fibers in particular polypropylene in this case. The kaolinite when stretched inside the fiber drawing deform by basal planes slipping rotating them and aligning this planes in between the polymer chains. The final result is a strong reinforcement of the fibers especially increasing their stiffness. The final goal is to characterize the composite polypropylene–kaolinite, their texture and the coupled deformation. This is done using fiber diffraction experiment with 2D images and working in transmission. One of the problems is that to perform this analysis by Rietveld texture-stress refinement we need to know exactly the starting structure and microstructure of both phases and in particular the kaolinite, its purity, the contaminant and its faulted structure. The kaolinite has a modulated disordered structure with the main stacking direction for the planar defects along the *c*-axis in the *P*1 space group. The disorder on the *c*-axis is modulated by the other two axes as shown by TEM (transmission electron microscope) selected area electron diffraction images (Kogure and Inoue, 2005).

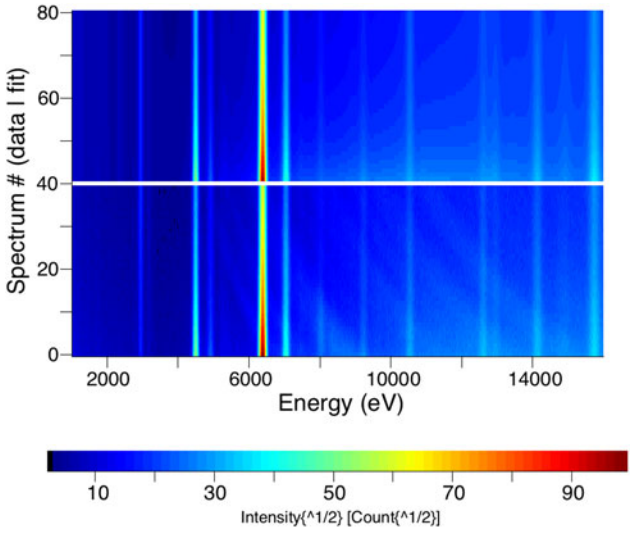

Figure 6. The 2D plot of the full XRF fit including the variation of the incident angle of the incoming beam. The incident angle was 10.5° for the first spectrum and about 49.5 for the last one. In the lower part the 40 experimental XRF spectra are reported and in the upper part the recalculated 40 ones are visible. Also, note the Cu diffraction line at 8 keV coming from the shutter as a non-continuous line.

The sample showed the presence of two phases, a disordered kaolinite and a small percentage of quartz. Both structures where used in the model to fit the XRD and XRF data simultaneously. The XRF showed the presence of several other elements as contaminant. Owing to the measurement done in air we could not check for the presence of Na or Mg impurities and we cannot report on them.

The final model was built by assuming all the impurities where in the kaolinite. Being the quartz <1%, putting them also in the quartz will not have changed the results significantly, and the opposite model with all impurities in the quartz is not reliable owing to the total amount of impurities.

To describe the kaolinite-modulated disordered structure we started from the pure turbostratic model described by a supercell approximation (Ufer *et al.*, 2004; Lutterotti *et al.*, 2009). We added to the model two modulation axes and we assumed no faults in the (*00l*) planes are detectable beyond the $l > 3$. The final fitting is visible in Figures 4–6. Figure 4 reports the XRD fitting where the planar disorder is visible only up to 20° and disappears after this is an effect of the modulation of the disorder in kaolinite. The XRF shows the string peaks of the Fe as well as some of the strange impurities such as Ga and Th. The thorium, even if is relatively abundant in the earth as a heavy element, is not a common element in these clay minerals, but we could not find any other element who could fit just this peak without other peaks were not detectable. We also check for escape or summation peaks, but it does not correspond. It should be noted that Figure 5 reports only the cumulative plot of all XRF spectra recorded at different incident beam angle but refined as separated spectra. In Figure 6, it is possible to compare the true experimental XRF data with the fitting. The figure shows the changes in intensities with the increasing penetration and consequently bigger absorption and some Bremsstrahlung diffracted reflections (the curved lines) that contributes to the background in Figure 5. In the present version of the software we do not calculate those lines, but we plan to do it in the future. The measurement and fitting of several XRF spectra for different incident beam angles are important to resolve in-depth composition gradients (not present here).

The results of the phase and elemental analysis are reported in Table II.

https://doi.org/10.1017/S0885715617000276 Published online by Cambridge University Press

TABLE II. Chemical and crystallographic quantitative analysis for the ceramic industry waste sample.

Phase				Kaolinite						Quartz					
wt%				99.6(5)						0.40(4)					
Element	O	Al	Si	Fe	Ti	Zr	Sr	Ce	Co	Ni	Ga	Cr	Y	Ca	Th
wt%	55.9	20.3	21.1	1.23	1.33	0.074	0.017	0.076	0.009	0.004	0.007	0.006	0.004	0.004	0.012

It is not possible to calculate the errors for elements below the silicon as their quantity is estimated from the crystallography of the phases.

V. CONCLUSION

A combined XRD/XRF characterization methodology has been presented. The technique consists of an approach integrated from both the experimental and analytical point of views. For what concerns the former, a combined XRD/XRF instrument has been used with a single X-ray Mo source and dedicated XRD/XRF detectors. From the analytical point of view, a Rietveld-like approach has been implemented, in which both the XRD and XRF data are being fitted starting from a unique structural model, described with a multi-phase mixture. We have shown how the combination of two sets of data coming from two different interactions of radiation with matter significantly increases the robustness and analytical capabilities of the two techniques, compared with their independent use. From the XRD point of view, the accuracy in chemical composition determination significantly increases, especially when dealing with substitutional impurities or amorphous phases; in addition, preliminary chemical information provided by XRF can also be optimally integrated into qualitative phase analysis (*search match*). From the XRF standpoint, the principal theoretical advantage of using a full crystallographic description of the sample is that the correct absorption of the fluorescence lines in the material can be calculated, allowing more precise matrix effect and consequently chemical composition calculations. Moreover, light elements (or, in general, elements outside the sensitivity range of the instrumentation) can be indirectly measured by detecting the corresponding element-bearing phases by means of XRD.

In general, the combined analysis paradigm allows a more reliable phase and chemical composition determination, since it is based on a single model complying in a best-fit sense with both diffraction and fluorescence datasets.

ACKNOWLEDGEMENT

The authors L. Lutterotti and M. Bortolotti wish to acknowledge the support of the European Project H2020 Solsa, Grant Agreement no. 689868.

De Voorde, L. V., Vekemans, B., Verhaeven, E., Tack, P., De Wolf, R., Garrevoet, J., Vandenabeele, P., and Vincze, L. (**2015**). "Analytical characterization of a new mobile X-ray fluorescence and X-ray diffraction instrument combined with a pigment identification case study," Spectrochim. Acta B **110**, 14–19.

Ebel, H. (**1999**). "X-ray Tube Spectra," X-ray Spectrom. **28**, 255–266.

Ingerle, D., Pepponi, G., Meirer, F., Wobrauschek, P., and Streli, C. (**2016**). "JGIXA – a software package for the calculation and fitting of grazing incidence X-ray fluorescence and X-ray reflectivity data for the characterization of nanometer-layers and ultra-shallow-implants," Spectrochim. Acta B **118**, 20–28.

Kerner, J. A., Franco, E. D., and Marshall, J. (**1995**). "Combined XRD and XRF analysis for portable and remote applications," Adv. X-Ray Anal. **38**, 319–324.

Kogure, T. and Inoue, A. (**2005**). "Determination of defect structures in kaolin minerals by high-resolution transmission electron microscopy (HRTEM)," Am. Mineral. **90**, 85–89.

Lutterotti, L. (**2010**). "Total pattern fitting for the combined size–strain–stress–texture determination in thin film diffraction", Nucl. Instrum. Methods Phys. Res. B **268**, 334–340.

Lutterotti, L., Bortolotti, M., Ischia, G., Lonardelli, I., and Wenk, H.-R. (**2007**). "Rietveld texture analysis from diffraction images," Z. Kristallogr. **26**, 125–130.

Lutterotti, L., Voltolini, M., Wenk, H.-R., Bandyopadhyay, K., and Vanorio, T. (**2009**). "Texture analysis of a turbostratically disordered Ca-montmorillonite," Am. Mineral. **95**, 98–103.

Pantos, E., Kockelmann, W., Chapon, L. C., Lutterotti, L., Bennet, S. L., Tobin, M. J., Mosselmans, J. F. W., Pradell, T., Salvado, N., Butí, S., Garner, R., and Prag, A. J. N. W. (**2005**). "Neutron and X-ray characterisation of the metallurgical properties of a 7th century BC Corinthian-type bronze helmet," Nucl. Instrum. Methods Phys. Res. B **239**, 16–26.

Rietveld, H. M. (**1967**). "Line profiles of neutron powder-diffraction peaks for structure refinement," Acta Crystallogr. **22**, 151–152.

Rietveld, H. M. (**1969**). "A profile refinement method for nuclear and magnetic structures," J. Appl. Crystallogr. **2**, 65–71.

Schönenberger, J., Momose, T., Wagner, B., Leong, W. H., and Tarnawski, V. R. (**2012**). "Canadian field soils I. Mineral composition by XRD/XRF measurements," Int. J. Thermophys. **33**, 342–362.

Ufer, K., Roth, G., Kleeberg, R., Stanjek, H., Dohrmann, R., and Bergmann, J. (**2004**). "Description of X-ray powder pattern of turbostratically disordered layer structures with a Rietveld compatible approach," Z. Kristallogr. **219**, 519–527.

Vaniman, D. T., Bish, D., Guthrie, G., Chipera, S., Blake, D. E., Collins, S. A., Elliott, S. T., and Sarrazin, P. (**1999**). "Process monitoring and control with CHEMIN, a miniaturized CCD-based instrument for simultaneous XRD/XRF analysis," Proc. SPIE Int. Soc. Opt. Eng. **3769**, 243–251.